Electronic Supplementary Material (ESI) for Nanoscale.

Supporting Information

High-Performance NO_2 Sensors Based on Spontaneously Functionalized Hexagonal Boron Nitride Nanosheets via Chemical Exfoliation

Yue He,[a] Dongdong Li,[a] Wei Gao,[a] Hong Yin,*[a] Fang Chen [b] and Yanfeng Sun [b]

[a]. State Key Lab of Superhard Materials, College of Physics, Jilin University, Changchun 130012, P. R. China. Email: hyin@jlu.edu.cn

[b]. State Key Laboratory on Integrated Optoelectronics, College of Electronic Science and Engineering, Jilin University, Changchun 130012, P. R. China.

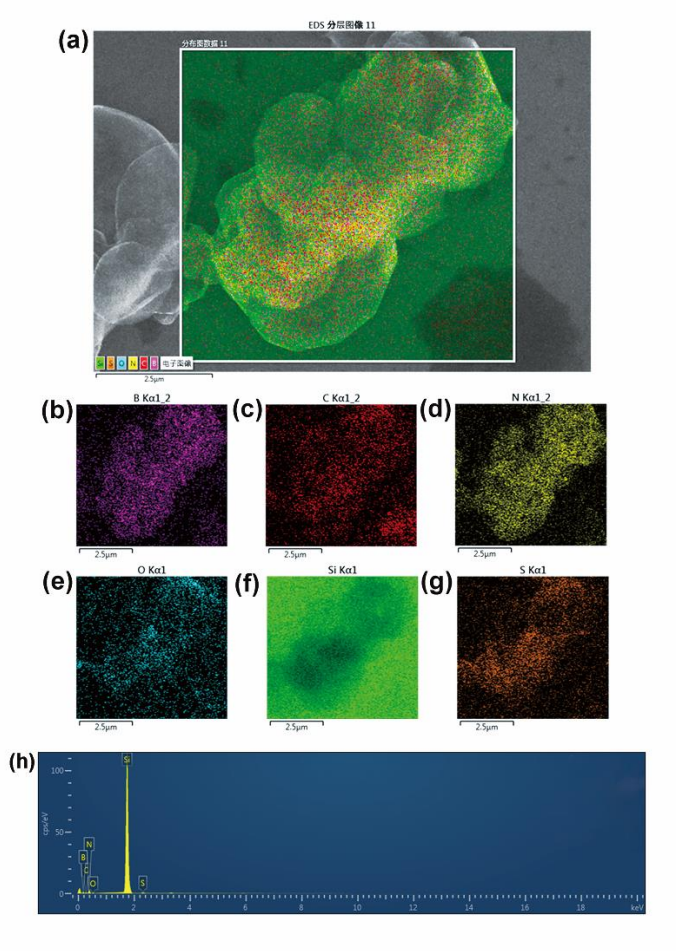

Fig. S1 EDX spectra analysis of S-BNNSs.

Table S1 The concentration of each element for S-BNNSs

Sample	Chemical composition (at. %)				
	B	N	C	O	S
S-BNNSs	62.34	22.88	13.35	1.31	0.12

In order to verify the presence of the sulfate groups, we performed an EDX test on S-BNNSs dispersed on a silicon (100) substrate. The resultant data are listed in Fig. S1 and Table S1. As shown in the Fig. S1, it can be clearly seen that B, N, C, O and S can be detected on the S-BNNSs area. Also, S distributes on the BN surface uniformly. The elemental compositions of B, N, C, O and S have been evaluated. Together with the XPS and FTIR, this indicates that the surfaces of BNNSs are successfully decorated by the sulfate group.

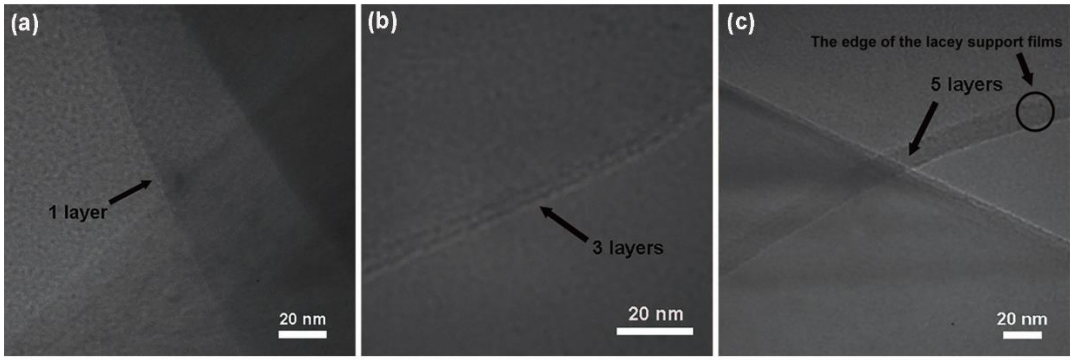

Fig. S2 Representative HRTEM images of S-BNNSs edges

In order to statistically estimate the thickness of the S-BNNSs, we measured the edges of the exfoliated nanosheets, since the edges of the individual sheets are almost always distinguishable in TEM images. We designate the sheet thickness as the layer number per sheet. By carefully counting the layer edges, it is possible to measure the number of layers per sheet. Certainly for some special cases, it is extremely difficult to recognize the edges. Thus it is expected the errors involved to be random and can be cancelled out when statistical results are analyzed in histogram. Fig. S2 shows several representative TEM images taken on the sheet edge.

As can be observed, the thickness of these nanosheets after exfoliation process ranges from monolayer to multiple layers. We use Gaussian distribution function to extract mean values for these data. It can be estimated that the mean thickness of these exfoliated h-BN nanosheets consist of three atomic layers (approximately 1.0 nm in thickness, considering 0.33 nm for one atomic layer).[1]

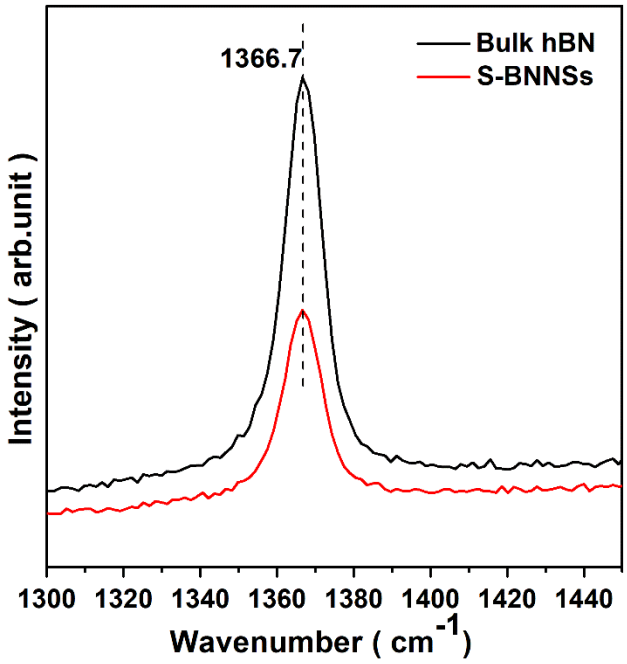

Fig. S3 Raman spectra of bulk h-BN (black) and S-BNNSs (red).

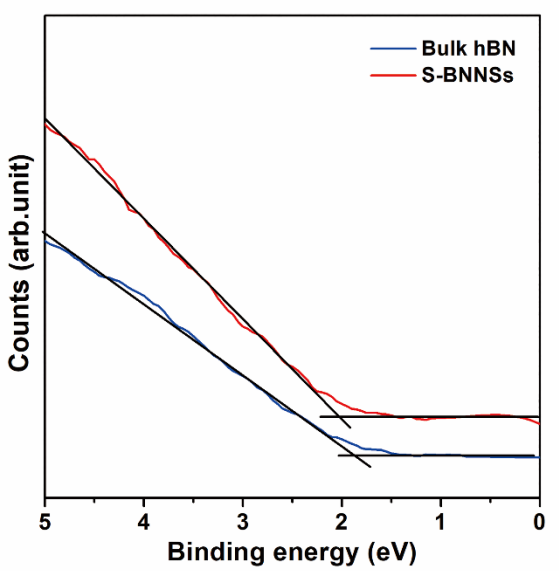

Fig. S4 XPS valence band spectra (VBS) of the bulk h-BN and S-BNNSs.

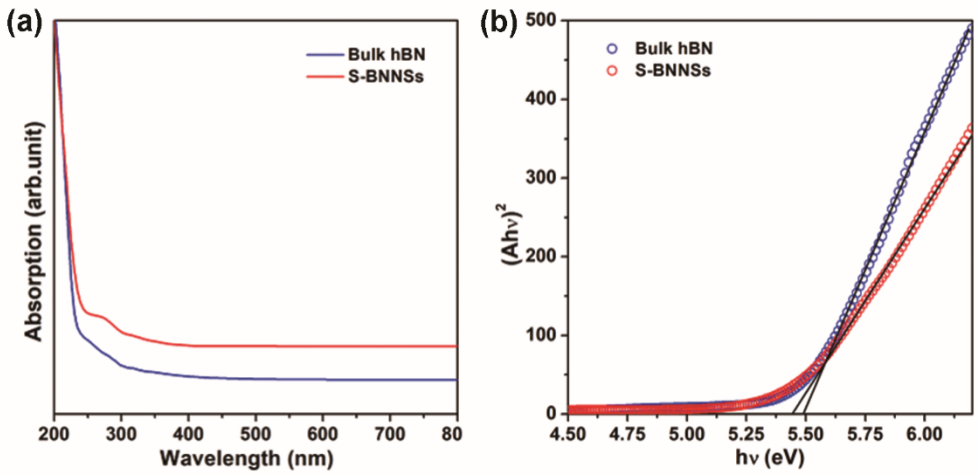

Fig. S5 UV-Vis spectra (a) and the Tauc plot (b) of the bulk h-BN and S-BNNSs.

The valence band spectral analysis (VBS) was obtained by executing XPS on bulk h-BN and S-BNNSs to confirm the energy band positions, as shown in Fig. S4. Bulk h-BN displays a valence band with the edge of the maximum (VBM) energy at about 1.87 eV, whereas the S-BNNSs sample exhibits a VBM energy at about 2.02 eV. The UV-Vis spectra are shown in Fig. S5. The absorption edge of bulk h-BN is about 237.6 nm, corresponding to the band gap of 5.49 eV. This is in the reasonable range of band gap observed in h-BN.[2] In comparison, the main absorption edge of S-BNNSs shifts to 246.5 nm, corresponding to a band gap of 5.44 eV. This is smaller than that of bulk h-BN,

which can be attributed to the existence of surface sulfate group. The new emerged absorption peak (277 nm) can be correlated with the opening of a mid-gap state in h-BN due to the addition of sulfate group modification.[3]

Combining the results of UV-Vis and VBS, the conduction band minimum (CBM) energy is -3.62 eV for the bulk h-BN. As far as the S-BNNSs, however, the CBM stays at -3.42 eV and shifts down by 0.2 eV, compared with that of bulk h-BN. Accordingly, the introduction of sulfate group in the present case moves down the whole bands. Furthermore, the VBM of S-BNNSs is shifted down by 0.15 eV due to the addition of sulfate group.

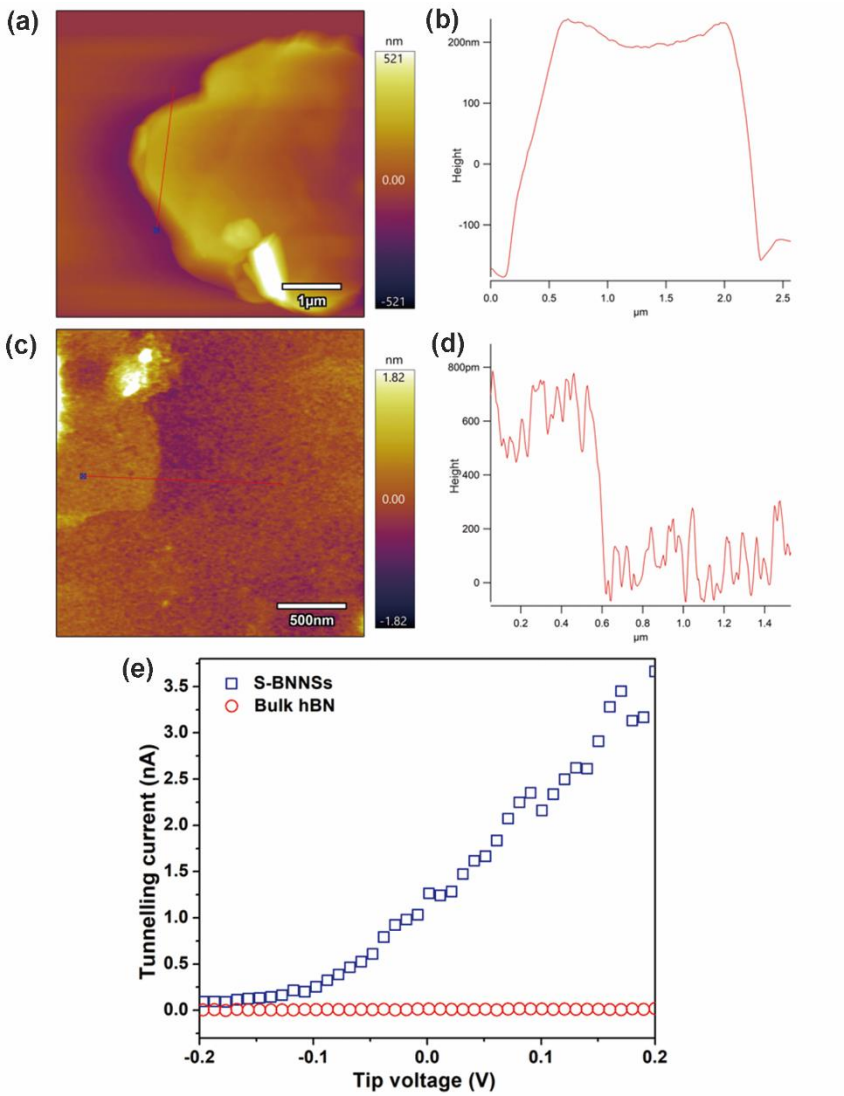

Fig. S6 Conductive atomic force microscopy (C-AFM) characterization of bulk h-BN and S-BNNSs. Topographic and the respective thickness profiles of bulk h-BN (a, b) and S-BNNSs (c,d), respectively. (e) I−V curves collected on bulk h-BN and S-BNNSs surfaces.

The C-AFM experiments were carried out in a Cypher ES Environmental AFM. We used a Ti/Ir varnished Si probes from Nanosensors (model: CONTPT) for this measurement. We first dispersed the sample in ethanol solution using a ratio of 1:200, and then drop it onto a 1 cm × 1 cm heavily doped n-type silicon (100) substrate for measurement. Here, the AFM measurements confirmed the two-dimensional nature of the S-BNNSs sample as shown in Fig. S6. The thicknesses of bulk h-BN and S-BNNSs are approximately 300 nm and 0.6 nm, respectively, which is consistent with our

previous statistical results for sample thickness. Thus, this representative S-BNNS sheet is comprised of approximately two atomic layers.

Fig. S6 (e) shows the I-V curves measured through Ti/Ir tip in contact of sample surface on silicon substrate in Fig. S6 (a) and (c). The current has been collected through the dispersed thin layer on the substrate. It can be clearly observed that within the range of -0.2V to 0.2V, the bulk h-BN shows negligible currents, indicating its highly electronic resistive nature. On the contrary, a current in the range of ~ nA is detected through the S-BNNSs sample, which is also linearly increased with the increasing voltage. Given approximately 3.5 nA current at a voltage of 0.2 V flowing across the S-BNNSs thin layer, the overall resistance of the S-BNNSs sample is estimated to be around 60 Mohm, which is sensibly in good agreement with the resistance values measured during the gas sensing test.

The different electrical properties of bulk h-BN and S-BNNSs have been confirmed. As known, the bulk h-BN is not beneficial in nature and cannot be applied in the field of gas sensors because of its high resistance. In the present work, the electronic property of S-BNNSs such as resistance is changed by surface grafting of sulfate group, which makes it possible to be applied in the field of gas sensors.

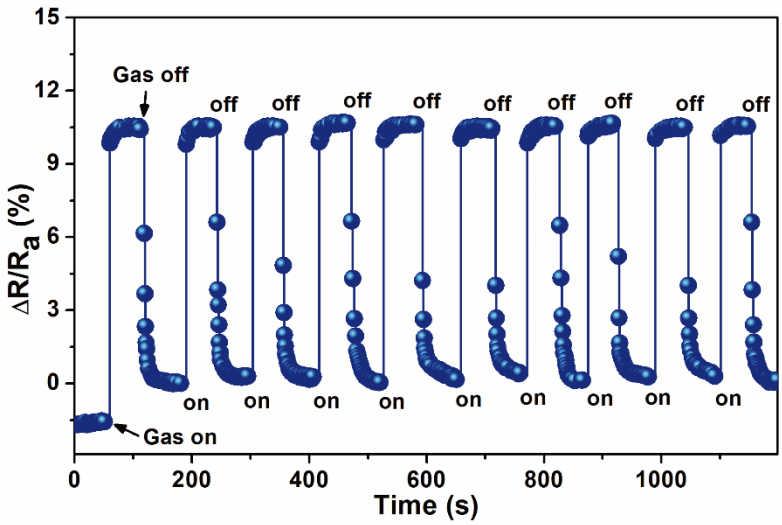

Fig. S7 Response of the S-BNNSs sensor to 10 ppm NO_2 in 10 successive cycles.

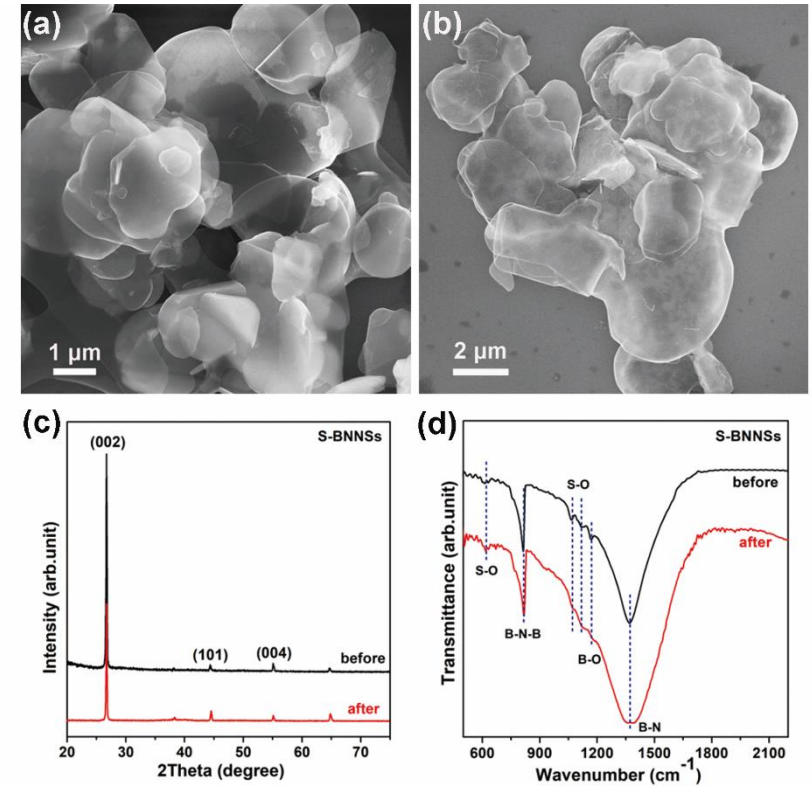

Fig. S8 (a) and (b) are SEM images of S-BNNSs before and after long-term operation, respectively. (c) and (d) are the XRD and FTIR spectra of S-BNNSs before and after long-term operation, respectively.

In order to prove the structural and morphological stability of S-BNNSs after long-term operation, SEM, XRD and FTIR have been used to characterize the S-BNNSs before and after sensing test to NO_2 gas in 10 successive cycles running for several times. The SEM images in Fig. S8 (a) and (b) illustrated that the surface morphology of S-BNNSs remains almost the same after long-term operation. XRD and FTIR measurements provide further information on the stability. As shown in Fig. S8 (c) and (d), the S-BNNSs sample preserve invariant even after sensing test to NO_2 gas in 10 successive cycles running for several times. Additionally, no extra treatments are necessary for re-using.

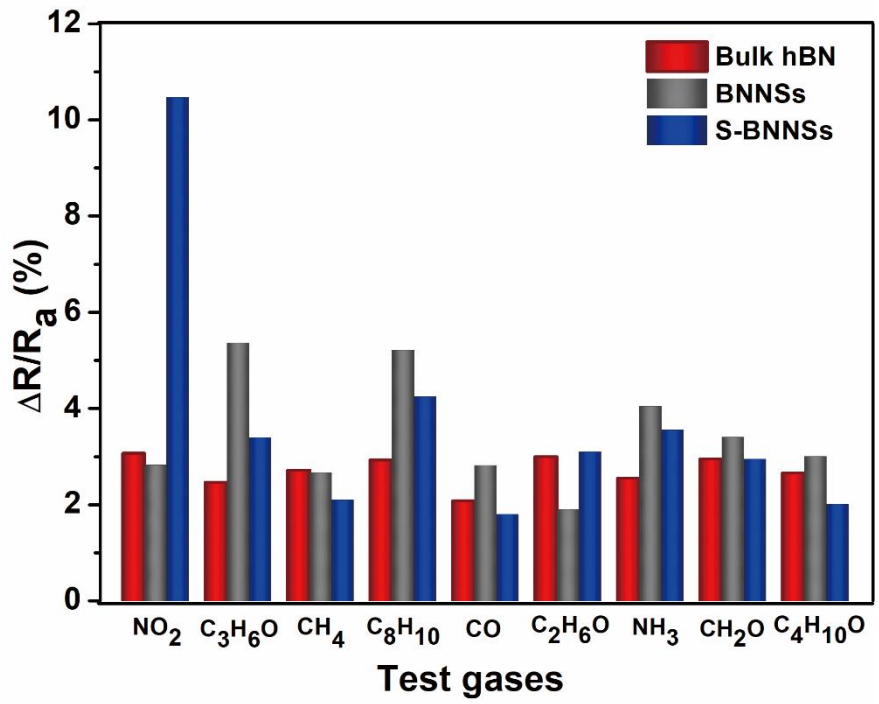

Fig. S9 Responses of the sensors based on S-BNNSs, unmodified BNNSs and bulk h-BN to various target gases.

We have tested the gas sensing performance of the bulk h-BN, BNNS and S-BNNSs to various gases, including methane (CH_4), carbon monoxide (CO), ammonia (NH_3), acetone (C_3H_6O), dimethylbenzene (C_8H_{10}), formaldehyde (CH_2O), ethanol (C_2H_6O), and butyl alcohol ($C_4H_{10}O$) in concentration of 100 ppm and 10 ppm NO_2 for comparison. As shown in Fig. S9, S-BNNSs-based sensor shows excellent selectivity towards NO_2, which highlights the positive role of sulfate groups in gas sensing. In comparison, the unmodified BNNSs and h-BN based sensors response nearly indiscernible to almost all the target gases.

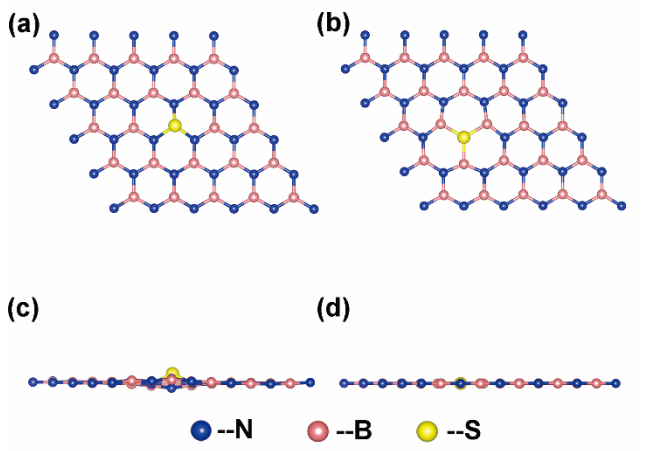

Fig. S10 The top view and side view of optimized structures of S_B-BNNS (a, c) and S_N-BNNS (b, d).

In DFT calculations of S-BNNSs, we modeled a 5×5 supercell of h-BN monoatomic layer (25 B and 25 N atoms) with a single S atom substituting either a B atom (denoted as S_B-BNNS) or an N atom (denoted as S_N-BNNS). The corresponding doping concentration is 2 %. This is reasonable since XPS measurements show that 30 boron atoms are functionalized by one sulfate (corresponding to 1.7 % doping concentration). Fig. S10 shows the optimized structures of S_B-BNNS and S_N-BNNS. By substituting the B atom with S atom, geometric structure of the BN sheet is distorted as illustrated in Fig. S10 (a, c). The S atom protrudes out of the planar, at a distance of 0.5953 Å from the sheet plane. As a consequence, after structural optimizing, the S-N bond length is enlarged from 1.437Å to 1.766Å. On contrary, the S_N-BNNS system retains planar form of the pure BNNS sheet (Fig. S10 (b,d)).

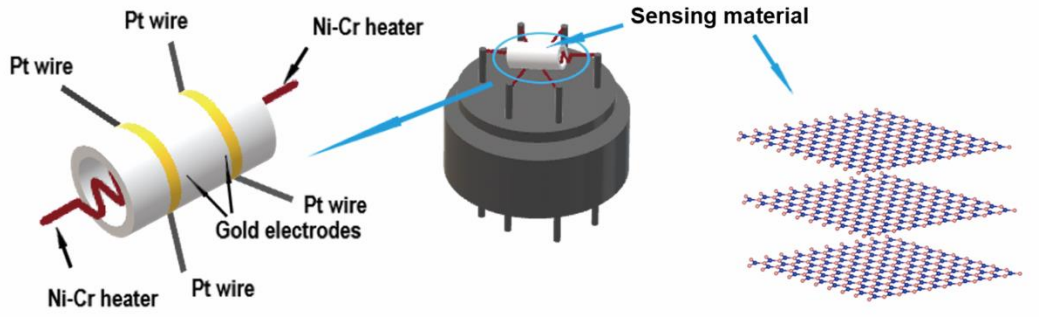

Fig. S11 The sensor structure and test component

Table S2 Sensing performance of various 2D materials-based NO_2 sensors

Sensing material	Response	Conc. [ppm]	Res/Rec time [s]	Experimental LOD [ppb]	Sensitivity	ref
mixed MoS_2 flakes	-10.36%	10	8.51/-	-	-	4
mixed MoS_2 flakes	-7.79%	10	4.44/19.6	-	-	4
mixed MoS_2 flakes	-21.78%	10	6.09/146.49	-	-	4
MoS_2/SnO_2	28%	10	>400/>160	500	-	5
graphene/MoS_2	-8%	5	-	1200	-	6
MoS_2/graphene	-8%	0.5	<60/<60	50	-	7
rGO/P NFs	1.03%	1	240/600	150	1.03	8
graphene	11%	5	300/600~720	5000	-	9
graphene nanomesh	4.32%	1	900/-	1000	-	10
3D Graphene flower	700%	6	>500/2	100	133.2	11
3D sulfonated RGO hydrogel	22.5%	2	12/11	200	8.69	12
sulfonated RGO	24.7	50	>500/>2000	5000	0.443	13
BNNSs	10.47%	10	7.5/14.4	20	1.645	this work

References

S1. L. H. Li and Y. Chen, *Adv. Funct. Mater.*, 2016, **26**, 2594-2608.

S2. K. Watanabe, T. Taniguchi and H. Kanda, *Nature Materials*, 2004, **3**, 404-409.

S3. G. R. Bhimanapati, D. Kozuch and J. A. Robinson, *Nanoscale*, 2014, **6**, 11671-11675.

S4. A. V. Agrawal, R. Kumar, S. Venkatesan, A. Zakhidov, G. Yang, J. Bao, M. Kumar and M. Kumar, *ACS Sensors*, 2018, **3**, 998-1004.

S5. S. Cui, Z. Wen, X. Huang, J. Chang and J. Chen, *Small*, 2015, **11**, 2305-2313.

S6. B. Cho, J. Yoon, S. K. Lim, A. R. Kim, D.-H. Kim, S.-G. Park, J.-D. Kwon, Y.-J. Lee, K.-H. Lee, B. H. Lee, H. C. Ko and M. G. Hahm, *ACS Applied Materials & Interfaces*, 2015, **7**, 16775-16780.

S7. H. Long, A. Harley-Trochimczyk, T. Pham, Z. Tang, T. Shi, A. Zettl, C. Carraro, M. A. Worsley and R. Maboudian, *Adv. Funct. Mater.*, 2016, **26**, 5158-5165.

S8. W. Yuan, L. Huang, Q. Zhou and G. Shi, *ACS Applied Materials & Interfaces*, 2014, **6**, 17003-17008.

S9. L. K. Randeniya, H. Shi, A. S. Barnard, J. Fang, P. J. Martin and K. Ostrikov, *Small*, 2013, **9**, 3993-3999.

S10. R. K. Paul, S. Badhulika, N. M. Saucedo and A. Mulchandani, *Anal. Chem.*, 2012, **84**, 8171-8178.

S11. J. Wu, S. Feng, X. Wei, J. Shen, W. Lu, H. Shi, K. Tao, S. Lu, T. Sun, L. Yu, C. Du, J. Miao and L. K. Norford, *Adv. Funct. Mater.*, 2016, **26**, 7462-7469.

S12. J. Wu, K. Tao, Y. Guo, Z. Li, X. Wang, Z. Luo, S. Feng, C. Du, D. Chen, J. Miao and L. K. Norford, *Advanced Science*, 2017, **4**, 1600319.

S13. W. Yuan, A. Liu, L. Huang, C. Li and G. Shi, *Adv. Mater.*, 2013, **25**, 766-771.